

Simulation of a partially depleted absorber (PDA) photodetector

Yue Hu,^{1,*} Thomas F. Carruthers,¹ Curtis R. Menyuk,¹
Meredith N. Hutchinson,² Vincent J. Urick,² and Keith J. Williams,²

¹Computer Science and Electrical Engineering Department,
University of Maryland Baltimore County, Baltimore, MD, 21250, USA

²Naval Research Laboratory, Photonics Technology Branch, Washington, DC 20375, USA

[*yuehu1@umbc.edu](mailto:yuehu1@umbc.edu)

Abstract: We use a 2D drift-diffusion model to study the nonlinear response of a partially depleted absorber (PDA) photodetector. The model includes external loading, incomplete ionization, the Franz-Keldysh effect, and history-dependent impact ionization. It also takes into account heat flow in the device. With all these effects included, we obtain excellent agreement with experiments for the responsivity and for the harmonic power at different modulation frequencies. The role of these different physical effects is elucidated, and we find that both the Franz-Keldysh effect and the load resistance play a key role in generating higher harmonic power at larger reverse biases. Increasing the size of the p -region absorption layers reduces the impact of the Franz-Keldysh effect. Decreasing the effective load resistance also decreases the higher harmonic powers. We also show that the model can suggest design changes that will improve device performance.

© 2015 Optical Society of America

OCIS codes: (040.5160) Photodetectors.

References and links

1. J. C. Campbell, A. Beling, M. Piels, Y. Fu, A. Cross, Q. Zhou, J. Peters, J. E. Bowers, and Z. Li, "High-power, high-linearity photodiodes for rf photonics," in 2012 Conference on Optoelectronic and Microelectronic Materials & Devices (COMMAD), (IEEE, Melbourne, 2012), pp. 215–216.
2. Y. Hu, C. Menyuk, V. Urick, and K. Williams, "Sources of nonlinearity in a pin photodetector at high applied reverse bias," in 2013 International Topical Meeting on Microwave Photonics (MWP), (IEEE, Alexandria, 2013), pp. 282–285.
3. Y. Hu and C. Menyuk, "Computational modeling of nonlinearity in a pin photodetector," in 2013 International Semiconductor Device Research Symposium (ISDRS), (Bethesda, 2013).
4. Y. Hu, B. Marks, C. Menyuk, V. Urick, and K. Williams, "Modeling sources of nonlinearity in a simple p-i-n photodetector," *J. Lightw. Technol.* **32**, 3710–3720 (2014).
5. D. A. Tulchinsky, X. Li, N. Li, S. Demiguel, J. C. Campbell, and K. J. Williams, "High-saturation current wide-bandwidth photodetectors," *IEEE J. Sel. Topics Quantum Electron.* **10**, 702–708 (2004).
6. A. S. Hastings, D. A. Tulchinsky, and K. J. Williams, "Photodetector nonlinearities due to voltage-dependent responsivity," *IEEE Photon. Technol. Lett.* **21**, 1642–1644 (2009).
7. A. S. Hastings, D. A. Tulchinsky, K. J. Williams, H. Pan, A. Beling, and J. C. Campbell, "Minimizing photodiode nonlinearities by compensating voltage-dependent responsivity effects," *J. Lightw. Technol.* **28**, 3329–3333 (2010).
8. R. McIntyre, "A new look at impact ionization-part I: A theory of gain, noise, breakdown probability, and frequency response," *IEEE Trans. Electron Devices*, **46**, 1623–1631 (1999).
9. P. Yuan, K. Anselm, C. Hu, H. Nie, C. Lenox, A. L. Holmes, B. Streetman, J. Campbell, and R. McIntyre, "A new look at impact ionization-Part II: Gain and noise in short avalanche photodiodes," *IEEE Trans. Electron Devices* **46**, 1632–1639 (1999).

10. Y. Fu, H. Pan, Z. Li, A. Beling, J. C. Campbell, "Characterizing and modeling nonlinear intermodulation distortions in modified uni-traveling carrier photodiodes," *IEEE J. Quantum Electron.* **47**, 1312–1319 (2011).
11. S. Selberherr, *Analysis and simulation of semiconductor devices* (Springer-Verlag, 1984).
12. D. C. Cole and J. Johnson, "Accounting for incomplete ionization in modeling silicon based semiconductor devices," in *Proceedings of the Workshop on Low Temperature Semiconductor Electronics*, (IEEE, Burlington, 1989), pp. 73–77.
13. F. Pfirsch and M. Ruff, "Note on charge conservation in the transient semiconductor equations," *IEEE Trans. Electron Devices* **40**, 2085–2087 (1993).
14. S. M. Sze and K. K. Ng, *Physics of semiconductor devices* (Wiley-Interscience, 2007). 3rd ed.
15. V. Palankovski, "Simulation of heterojunction bipolar transistors," PhD Dissertation, Technische Universität Wien, Vienna, Austria (2000).
16. M. Wagner, "Simulation of thermoelectric devices," PhD Dissertation, Technische Universität Wien, Vienna, Austria (2007).
17. M. Sotoodeh, A. H. Khalid, and A. A. Rezazadeh, "Empirical low-field mobility model for III-V compounds applicable in device simulation codes," *J. Appl. Phys.* **87**, 2890–2900 (2000).
18. R. Quay, "Analysis and simulation of high electron mobility transistors," PhD dissertation, Technische Universität Wien, Vienna, Austria (2001).
19. R. Quay, C. Moglestue, V. Palankovski, and S. Selberherr, "A temperature dependent model for the saturation velocity in semiconductor materials," *Mater. Sci. Semicond. Process.* **3**, 149–155 (2000).
20. J. Callaway, "Optical absorption in an electric field," *Phys. Rev.* **130**, 549–553 (1963).
21. K. Yang, J. C. Cowles, J. R. East, and G. I. Haddad, "Theoretical and experimental dc characterization of InGaAs-based abrupt emitter HBT's," *IEEE Trans. Electron Devices* **42**, 1047–1058 (1995).
22. K. Anselm, H. Nie, C. Hu, C. Lenox, P. Yuan, G. Kinsey, J. Campbell, and B. Streetman, "Performance of thin separate absorption, charge, and multiplication avalanche photodiodes," *IEEE J. Quantum Electron.* **34**, 482–490 (1998).
23. P. Yuan, C. Hansing, K. A. Anselm, C. V. Lenox, H. Nie, J. Holmes, A.L., B. Streetman, and J. Campbell, "Impact ionization characteristics of III-V semiconductors for a wide range of multiplication region thicknesses," *IEEE J. Quantum Electron.* **36**, 198–204 (2000).
24. M. A. Saleh, M. Hayat, P. Sotiirelis, A. Holmes, J. C. Campbell, B. Saleh, and M. Teich, "Impact-ionization and noise characteristics of thin III-V avalanche photodiodes," *IEEE Trans. Electron Devices* **48**, 2722–2731 (2001).
25. M. N. Draa, A. S. Hastings, and K. J. Williams, "Comparison of photodiode nonlinearity measurement systems," *Opt. Express* **19**, 12635–12645 (2011).
26. K. Tharmalingam, "Optical absorption in the presence of a uniform field," *Phys. Rev.* **130**, 2204–2206 (1963).

1. Introduction

High-power photodetectors play an important role in RF-photonics systems [1]. Nonlinearity in the photodetector leads to power generation at harmonics of the input signal frequencies, which limits the performance of these systems. We have studied the source of nonlinearity in a simple *p-i-n* photodetector [2–4], and we have found that impact ionization plays an important role in generating higher harmonic powers at high applied bias. We extend the model to study the sources of nonlinearity in a partially depleted absorber (PDA) photodetector [5], which has several absorption layers on each side of intrinsic region in PDA photodetector [5]. These photodetectors can support higher currents than can standard *p-i-n* photodetectors but have a structure that is significantly more complex. In InGaAs, the electron velocity is much greater than the hole velocity; the carrier velocity difference induces device nonlinearity. In a PDA photodetector, it is possible to have a better carrier balance in the intrinsic region, reducing the built-in fields, by adjusting the length of the absorption layers. While our simulation study focuses on a particular device structure [5], the issues that we discuss and our conclusions should be valid for a wider range of PDA photodetectors.

Subsequent to the original experimental study [5], it was discovered that several voltage-dependent effects, such as the Franz-Keldysh effect and impact ionization, play a role in the generation of higher harmonic power [6, 7]. In this work, we use a 2D drift-diffusion model that uses one longitudinal and one radial dimension and assumes cylindrical symmetry. It has been shown in prior work that a 2D model produces more reliable results than a 1D purely longitudinal model, particularly at low reverse bias where transverse current flow is important [4]. It also

allows us to avoid *ad hoc* assumptions for the radial intensity profile of the incident light. We include incomplete ionization, the Franz-Keldysh effect, external loading, and history-dependent impact ionization in our model [2–4, 8, 9], and we study the influence of all these effects on the harmonic power.

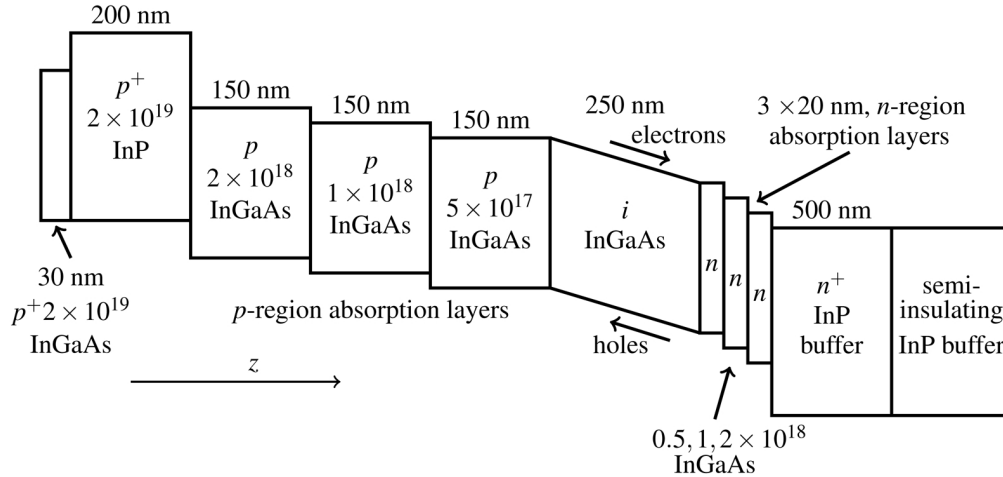


Fig. 1. Structure of PDA photodetector. Not drawn to scale.

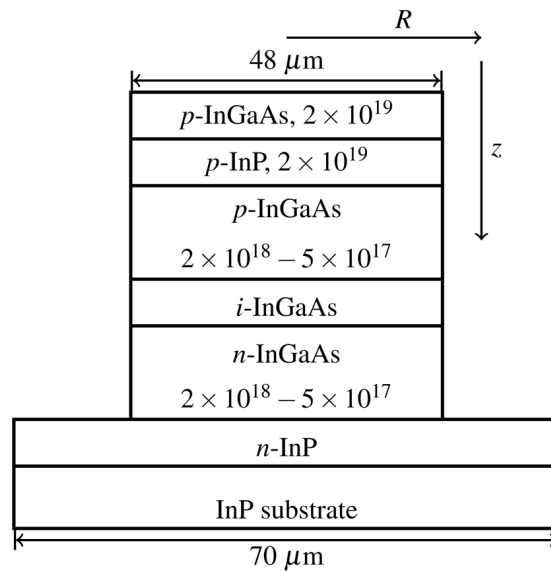


Fig. 2. The epitaxial structure of the modeled PDA photodetector. The pillar has a diameter of $48 \mu\text{m}$, and the base has a diameter of $70 \mu\text{m}$. Light is incident from the InP substrate side. Lengths are not to scale.

We will show that the Franz-Keldysh effect can be an important source of nonlinearity in PDA photodetectors. It leads to changes in the absorption coefficient that depend on the incident light wavelength and the strength of the electric field. Fu *et al.* [10] also found that the Franz-Keldysh effect is important in a MUTC photodiode. We will show that increasing the

length of the p -region absorption layers can eliminate the impact of the Franz-Keldysh effect. We also find that it is necessary to take into account the history dependence of the impact ionization in order to accurately calculate it. The “dead length” [9], which is the distance required for a carrier to gain sufficient kinetic energy from the electric field so that it can initiate impact ionization, cannot be ignored in devices like PDA photodetectors that have thin intrinsic regions. Finally, we will show that decreasing the effective load resistance decreases the harmonic powers.

The remainder of this paper is organized as follows: Section 2 contains a discussion of our photodetector model. Section 3 describes the simulation procedure and the experimental setup. Section 4 contains our simulation results. Section 5 discusses the effect of varying the device parameter. Section 6 contains the conclusions.

2. PDA photodetector model

2.1. Drift-diffusion model

To study carrier transport in the photodetector, we model a PDA photodetector in two dimensions, longitudinal and radial, using the 2D drift-diffusion equations [2, 4, 11–13] with the configuration of Figs. 1 and 2, coupled with the heat flow equation. Compared with the p - i - n photodetector that was studied in [4], the temperature increases quickly in the PDA photodetector, because its electric field is higher than that in a p - i - n photodetector due to its thinner intrinsic layer. The output photocurrent in the experiment is also higher than in [4]. Additionally, we consider here a history-dependent impact ionization, which is important in a thin-intrinsic-layer device, but was not important to model the device in [4]. The model consists of three equations that govern the dynamics of the electron density n , the hole density p , and the electric field \mathbf{E} (negative gradient of the electrostatic potential, φ),

$$\frac{\partial (n - N_D^+)}{\partial t} = G_i + G_L - R(n, p) + \frac{\nabla \cdot \mathbf{J}_n}{q}, \quad (1a)$$

$$\frac{\partial (p - N_A^-)}{\partial t} = G_i + G_L - R(n, p) - \frac{\nabla \cdot \mathbf{J}_p}{q}, \quad (1b)$$

$$\nabla \cdot \mathbf{E} = \frac{q}{\epsilon} (N_D^+ + p - n - N_A^-), \quad (1c)$$

where q is the unit of charge (here positive), G_i and G_L are the impact ionization and photon generation rates, R is the recombination rate, ϵ is the permittivity of the semiconductor material, and N_D^+ and N_A^- are the ionized donor and acceptor impurity concentrations. The variables \mathbf{J}_n and \mathbf{J}_p are the current densities for electrons and holes, and are given by

$$\mathbf{J}_n = qn\mathbf{v}_n(\mathbf{E}) + qD_n\nabla n, \quad (2a)$$

$$\mathbf{J}_p = qp\mathbf{v}_p(\mathbf{E}) - qD_p\nabla p, \quad (2b)$$

where D_n and D_p are the electron and hole diffusion coefficients [4], respectively, while $\mathbf{v}_n(\mathbf{E})$ and $\mathbf{v}_p(\mathbf{E})$ are the electric-field-dependent electron and hole drift velocities [4], respectively.

The photon generation rate is given by [14]

$$G_L = Q\alpha(\omega, E)\exp[-\alpha(\omega, E)(L_{\text{ab}} - z)], \quad (3)$$

where Q is the incident photon flux entering the device, $\alpha(\omega, E)$ is the absorption coefficient as a function of the incident light frequency ω and the magnitude of the electric field E , L_{ab} is the length from the p -region to the end of the n -region absorption layers, and z is the distance to the top of the p -region. In the simulation, only single-pass illumination is considered.

We also include the temperature change that occurs due to heat that is generated by the device current and recombination. The heat flow equation [11, 15, 16] that governs the heat transport may be written as

$$\rho c_p \frac{\partial T}{\partial t} = (\mathbf{J}_n + \mathbf{J}_p) \cdot \mathbf{E} + R \cdot E_g + \nabla \cdot [k(T) \nabla T], \quad (4)$$

where ρ and c_p are the specific mass density and specific heat of the material, T is the lattice temperature, E_g is the energy gap of the material, and k is the thermal conductivity. The thermal conductivity may be expressed as [15]

$$k(T) = k_{300} \left(\frac{T}{300} \right)^{\alpha_k}, \quad (5)$$

where $k_{300} = 4.82$ W/K-m and α_k equals -1.17 in $\text{In}_{0.53}\text{Ga}_{0.47}\text{As}$. The electron and hole mobility and the energy gap of the material are functions of temperature; so, the heat flow equation must be included in the simulation. We solve the drift-diffusion equation and the heat flow equation iteratively to obtain the temperature distribution in the device at steady state.

We calculate the band-gap E_g , from the expression [11, 17, 18]

$$E_g(T) = 0.795 - \frac{4.91 \times 10^{-4} T^2}{301 + T}. \quad (6)$$

The low-field mobility is given by

$$\mu_n^L = \mu_{n,300}^L (T/300)^{r_n}, \quad \mu_p^L = \mu_{p,300}^L (T/300)^{r_p}. \quad (7)$$

For material A_xB_{1-x} , the mobility is expressed as [18]

$$\frac{1}{\mu_{AB}} = \frac{x}{\mu_A} + \frac{1-x}{\mu_B} + \frac{x(1-x)}{C_\mu}, \quad (8)$$

where C_μ equals 1×10^6 $\text{cm}^2/(\text{V}\cdot\text{s})$ for $\text{In}_x\text{Ga}_{1-x}\text{As}$. We show the low-field mobilities in Table 1 [14, 17, 18]. At room temperature, the electron mobility in $\text{In}_{0.53}\text{Ga}_{0.47}\text{As}$ equals 1.4×10^4 $\text{cm}^2/(\text{V}\cdot\text{s})$, and the hole mobility equals 300 $\text{cm}^2/(\text{V}\cdot\text{s})$.

Table 1. Material mobility parameters used in the simulation.

Material	$\mu_{n,300}^L$, $\text{cm}^2/(\text{V}\cdot\text{s})$	r_n	$\mu_{p,300}^L$, $\text{cm}^2/(\text{V}\cdot\text{s})$	r_p
GaAs	8500	-2.2	491.5	-0.9
InAs	32500	-1.7	530	-2.3
InP	5300	-1.9	200	-1.2

The saturated velocities of the holes and electrons are also functions of temperature. These functions may be written [19]

$$v_{n,\text{sat}}(T) = \frac{v_{n,\text{sat},300}}{(1 - A_n) + A_n T/300}, \quad v_{p,\text{sat}}(T) = \frac{v_{p,\text{sat},300}}{(1 - A_n) + A_n T/300}, \quad (9)$$

where A_n equals 0.56 for $\text{In}_{0.53}\text{Ga}_{0.47}\text{As}$. The saturated, room-temperature electron and hole velocities that we use in our simulations are 1.2×10^7 cm/s and 0.5×10^7 cm/s , respectively.

We use the same boundary condition as in [4]. We assume that the p - and n -contacts are ohmic contacts and offer no barrier to carrier flow. The electrostatic potential boundary conditions relate the given reverse bias V_a , the built-in potential V_{bi} , output photocurrent I , and load resistance R_{load} . We set the electrostatic potential at the p -contact to zero, such that the potential at the n -contact ϕ_n is

$$\phi_n = V_a - IR_{load} + V_{bi}. \quad (10)$$

The electric field is the negative gradient of the electrostatic potential.

2.2. Franz-Keldysh effect

When the photon energy of the incident optical light is close to the band edge of the InGaAs absorber, the Franz-Keldysh effect must be taken into account [10, 20]. More details on our model of the Franz-Keldysh effect can be found in [4]. The model of the Franz-Keldysh effect that we are using here does not include Coulomb interactions. We have found that these interactions must be taken into account when the light wavelength reaches 1580 nm for this particular structure. For a wavelength of 1550 nm, which we are considering here, their effect is small. We will discuss this issue in more detail elsewhere.

2.3. Impact ionization

Impact ionization is also an important source of nonlinearity in the photodetector [2, 4]. It can lead to an important increase in the electron and hole densities. We may write the electron and hole generation rate G_i as

$$G_i = \alpha_n \frac{|\mathbf{J}_n|}{q} + \alpha_p \frac{|\mathbf{J}_p|}{q}, \quad (11)$$

where α_n and α_p are the impact ionization coefficients of the electrons and holes, respectively. Only electron impact ionization is considered, because the electron impact ionization coefficient is at least an order of magnitude larger than the hole impact ionization coefficient in $\text{In}_{0.53}\text{Ga}_{0.47}\text{As}$. We calculate α_n using the formula [21]:

$$\alpha_n(E) = 6.64 \times 10^7 \exp\left(-2 \times 10^6/E\right). \quad (12)$$

Equation (12) assumes that the ionization coefficient of electrons is only a function of the local electric field; this assumption will become inaccurate in thin layers. A carrier has to gain enough energy from the electric field to have an ionizing collision [8, 9]. With a decrease of the material thickness, the impact ionization coefficient should decrease [22]. In order to cause ionization, an electron must travel a finite distance, which is frequently referred to as the “dead length,” before it can gain sufficient energy from the electric field to lead to a non-negligible ionization probability [23, 24]. In a thin device, this dead length cannot be ignored. We use

$$\alpha_n(x'|x) = 6.64 \times 10^7 \exp\left[-2 \times 10^6/E_{\text{eff},e}(x'|x)\right], \quad (13)$$

as a history-dependent ionization coefficient [9, 23] in the simulation, where $E_{\text{eff},e}$ is defined as the average of the electric field in a neighborhood $[x, x']$,

$$E_{\text{eff},e}(x'|x) = \int_x^{x'} dx'' E(x'') R_e(x''|x). \quad (14)$$

The correlation function R_e is given by

$$R_e(x''|x) = \frac{2}{\sqrt{\pi}\lambda_e} \exp\left[-\frac{(x''-x)^2}{\lambda_e^2}\right], \quad (15)$$

where λ_e is the correlation length, expressed in terms of the voltage drops across the dead length V_{de} . In the simulation, we use $\lambda_e = V_{de}/E$, and we set V_{de} equal to 4 V as in the experiments in [23].

3. Simulation procedure and experimental setup

For each bias voltage and optical power, we first solve the drift-diffusion [2, 4, 11–13] and heat flow equation [11, 15, 16] simultaneously to obtain the steady state. In order to investigate the sources of nonlinearity in the device, light that is modulated with a sine wave illuminates the device for a number of cycles (typically 10) until a steady output is obtained. The light generation in the device may be described as

$$G_t(t) = G_L \times [1 + m \sin(\omega_m t)], \quad (16)$$

where G_L is the steady state generation, m is the modulation depth, and ω_m is the modulation frequency. At each time step, we record the photocurrent. We then take the Fourier transform of the output current to obtain the harmonic power. In several cases, we carried the simulations out to 20 cycles and observed no significant difference in the results.

We use nearly the same computational model as in [4]. When discretizing the drift-diffusion equation, we use an even mesh in the R -direction with a step size of 0.5 μm . We use an uneven mesh in the z -direction, whose step sizes vary between 1 and 5 nm. We use a fine mesh when the electric field changes quickly, and a coarse mesh when electric field changes slowly. We use a fixed time step of 2×10^{-9} s. To obtain the data in the 2D simulation, we used 18 hours of time on UMBC's High Performance Computing Facility (HPCF) [<http://www.umbc.edu/hpcf>].

In the experiments that we are modeling [5], the responsivity was measured with backside illumination using an SMF fiber with an 8- μm core diameter that was backed off to fill the device active area more evenly. In the calculation, we choose a 12- μm Gaussian radius, which corresponds closely to the illumination radius in the experiment. The experimental harmonic data was taken using a one-tone heterodyne setup as described in [25]. The load resistance in the RF measurement was 50 Ω .

4. Simulation results

4.1. Device temperature

Figure 3 shows the temperature in the device with a bias of 5 V. In the middle of the device, the temperature can reach as high as 370 K. The most important parameter in the device that affects the harmonic power is the InGaAs band gap. The most important region of light absorption in the device that affects the harmonic power is the intrinsic region. We calculate the average temperature in the region of the device where the light is absorbed ($z = 0.2 - 1.3 \mu\text{m}$). We then use this average temperature to calculate the bandgap E_g and obtain the temperature dependent parameters that are used in the transient calculations.

Figure 4 shows the average temperature in the light-absorption region as a function of bias. When the bias increases, the temperature increases, leading to the decrease in the band gap. The velocities of the electrons and holes are also affected. We observe that the temperature change is only 30 K when the bias increases from 2 to 5 V; however, the energy gap decreases by 0.012 eV. Without considering the temperature increase, we cannot achieve agreement with the experiments.

4.2. Responsivity

Figure 5 shows the simulated and measured responsivity for a 9 mA output current. We obtain good agreement with the experimental results. In the simulation, incomplete ionization, impact

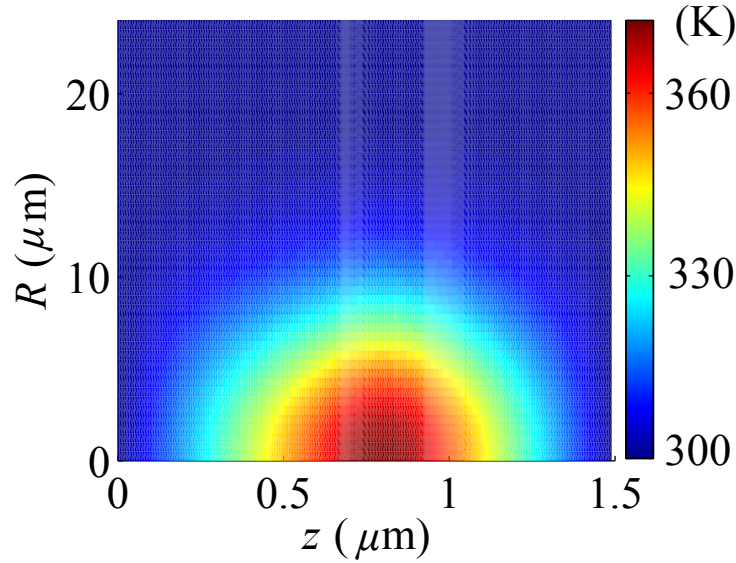


Fig. 3. Calculated temperature in the device. The bias is 5 V and the photocurrent is 10 mA.

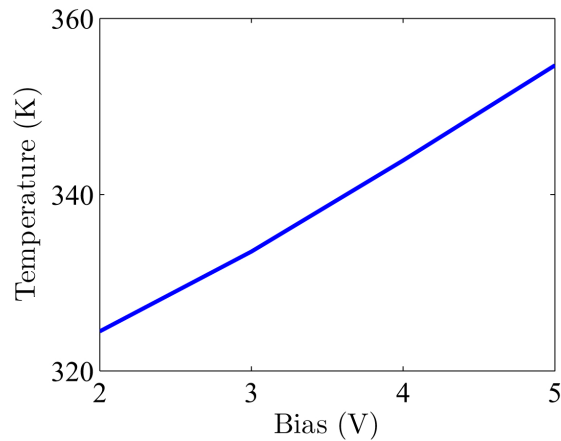


Fig. 4. Calculated average temperature in the device. The output photocurrent is 10 mA.

ionization, and an external load are kept. We then calculate the harmonic power using the same parameters. The parameters used in the simulations are shown in Table 2.

4.3. Harmonic power

Figure 6(a) shows the simulation results for the harmonic powers in the 1D simulation. The effective radius used in the simulation is $10 \mu\text{m}$. We obtain good agreement with the experiments. Figure 6(b) shows the calculated harmonic powers in the 2D simulation. Here we achieved excellent agreement with the experiments for all reverse biases. We include external loading, impact ionization, and the Franz-Keldysh effect in the simulation. The photocurrent is 10 mA, the modulation depth is 40%, and the modulation frequency is 2 GHz. The 2D simulation yields noticeably more accurate results than does the 1D simulation.

Table 2. Parameters used in the simulation at room temperature.

Parameter		
Electron mobility in InP	$\mu_{n,300}^L$	5300 cm ² /V-s
Electron mobility in InGaAs	$\mu_{n,300}^L$	14000 cm ² /V-s
Hole mobility in InP	$\mu_{p,300}^L$	200 cm ² /V-s
Hole mobility in InGaAs	$\mu_{p,300}^L$	300 cm ² /V-s
Electron saturated velocity	$v_{n,sat,300}$	1.2×10^7 cm/s
Hole saturated velocity	$v_{p,sat,300}$	5×10^6 cm/s
Permittivity	ϵ	1.21×10^{-12} F/cm
Electron velocity fitting parameter in InP	β	0.8×10^{-8} cm ² /V ²
Electron velocity fitting parameter in InGaAs	β	0.4×10^{-7} cm ² /V ²
Hole velocity fitting parameter	γ	2
Intrinsic region recombination times	τ_n, τ_p	20 ns
Doped regions recombination times	τ_n, τ_p	200 ps
Optical beam Gaussian radius	r_g	12 μ m
Radius of the device	R	24 μ m
Donor energy level	ΔE_D	0.025 eV
Acceptor energy level	ΔE_A	0.005 eV
Light wavelength	λ	1550 nm
Electron effective mass	m_n^*/m_0	0.041
Heavy hole effective mass	m_p^*/m_0	0.43
Light hole effective mass	m_p^*/m_0	0.04
InGaAs Band gap energy at 300 K	E_g	0.72 eV

Figure 7 shows the harmonic powers in the 2D simulation at the light modulation frequencies of 3.1 GHz and 4.3 GHz. We obtain excellent agreement with different modulation frequencies. We find that the fundamental power decreases when the frequency increases. This decrease occurs because the carriers respond less well to changes in the incident light as the frequency increases. The second harmonic power decreases more slowly when the frequency increases. The dip in the third harmonic power shifts from 4.0 V to 4.5 V when the frequency increases from 2.0 GHz to 3.1 GHz.

Figure 8(a) shows the influence of the Franz-Keldysh effect on the harmonic power as a function of the reverse bias. When the Franz-Keldysh effect is not kept in the simulation, the second and third harmonic powers in the simulation are smaller than the experimentally measured harmonic powers in the range from 2 V to 4 V. This result implies that the Franz-Keldysh effect is an important source of nonlinearity in the photodetector. Without the Franz-Keldysh effect, the harmonic powers decrease as the bias increases. However, with the Franz-Keldysh effect, the harmonic powers oscillate. We observe a dip in the third harmonic power when the bias is close to 4 V.

Photogenerated carriers change the electric field and hence the absorption coefficient, which

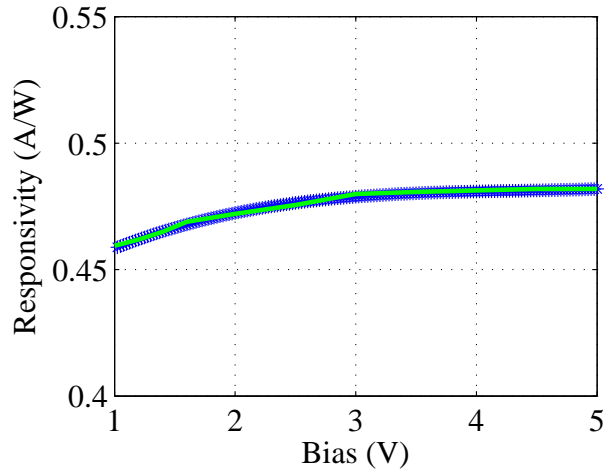


Fig. 5. Calculated responsivity of the photodetector in our 2D simulation. The blue symbols show the experimental results, and the green curve shows the simulated result. The output photocurrent is 9 mA. The incident light wavelength is 1550 nm.

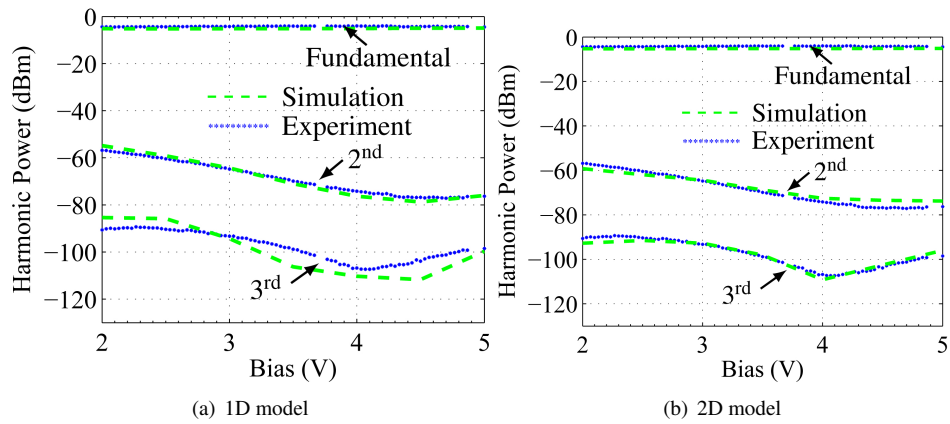


Fig. 6. Calculated harmonic powers of the photodetector output power in our 1D and 2D simulations. The symbols show the experimental data for the fundamental, second, and third harmonic powers. The dashed lines show the simulation results. The photocurrent is 10 mA, and the modulation depth is 40%. The modulation frequency is 2 GHz.

leads to changes in the output photocurrent. Due to the load resistor in the circuit, the voltage across the device changes so that the electric field in the device changes. When the load resistance is zero, Fig. 8(b) shows the harmonic powers with and without the Franz-Keldysh effect. Without the load resistor in the measured circuit, the voltage across the device is determined by the applied voltage. The electric field in the intrinsic region only changes slightly due to the change of the absorption coefficient. So, the Franz-Keldysh effect by itself makes little difference. It is the load resistor combined with the Franz-Keldysh effect that is the source of nonlinearity in the photodetector.

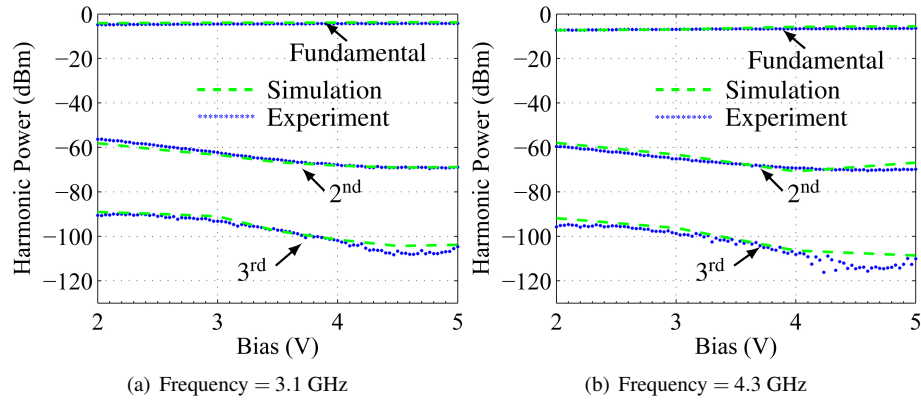


Fig. 7. Calculated harmonic powers of the photodetector output power in our 2D simulations. The symbols show the experimental data for the fundamental, second, and third harmonic powers. The curves show the simulation results. The photocurrent is 10 mA, and the modulation depth is 40%.

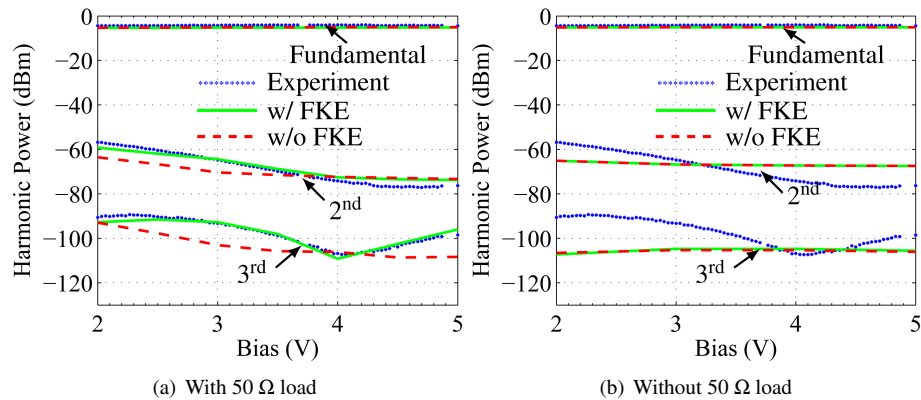


Fig. 8. Calculated harmonic powers of the photodetector output power in our simulations. The symbols show the experimental data for the fundamental, second, and third harmonic powers. The curves show the simulation results. The photocurrent is 10 mA, the modulation depth is 40%, and the modulation frequency is 2 GHz. The green solid curves show the simulation results with the Franz-Keldysh effect (FKE), and the red dashed curves show the simulation results without the Franz-Keldysh effect.

5. Parameter study

5.1. Impact of the base radius

Figure 9 shows the harmonic powers for different geometries of the photodetector. The green curves represent the simulation results with the structure shown in Fig. 2, in which the radius of the bottom layer (n -InP layer) of the device is larger ($35 \mu\text{m}$) than other layers ($24 \mu\text{m}$), and the red curves represent a uniform device, in which we assume that all layers in the device, including the base, have the same radius ($24 \mu\text{m}$). The simulation results show that changing the size of the base does not make much difference. The reason for this similarity is that the nonlinearity is primarily created in the p - and intrinsic layers. The real device has a large radius in the bottom layer. Here, we show that changing the base does not change the harmonic powers.

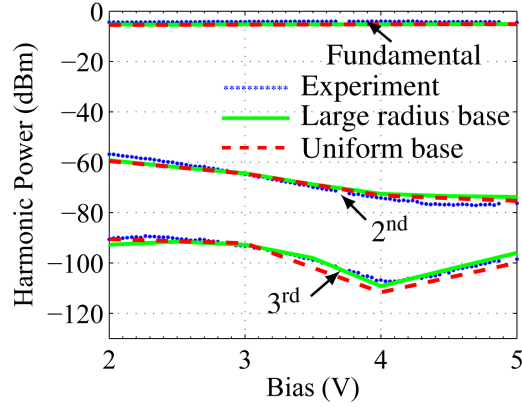


Fig. 9. Calculated harmonic powers of the photodetector output power in our 2D simulations. The symbols show the experimental data for the fundamental, second, and third harmonic power. The green solid curves show the simulation results when the base has a larger radius (green) and the same radius (red) as the other layers in the device. The photocurrent is 10 mA, the modulation depth is 40%, and the modulation frequency is 2 GHz.

Hence, we can use a relatively simple structure to calculate the harmonic powers in the device.

The actual device that we are modeling is not cylindrically symmetric, as we assume in our 2D simulations. Instead, it sits on a pedestal with the electrical contact on one side of the device. A full 3D simulation that models the actual geometry is too computationally time-consuming to allow us to carry out parameter studies. This result, which indicates that the behavior is largely independent of the geometry of the base, increases our confidence in the 2D simulations.

5.2. Validation of the Franz-Keldysh effect model

The Franz-Keldysh effect is a spatially extended effect that is due to tunneling of electrons through a barrier [20]. Here, we verify that the change in the field is small over the spatial extent of the Franz-Keldysh effect and will not affect the calculation of this effect. In order for the change in the field to be sufficiently small, the absorption length due to the Franz-Keldysh effect l_A should satisfy the condition

$$\frac{1}{l_A} \gg \max \left| \frac{1}{E} \frac{dE}{dz} \right|, \quad (17)$$

where

$$l_A = \left(\frac{\hbar^2}{2e\mu E} \right)^{1/3}. \quad (18)$$

The absorption coefficient is obtained from a dimensional analysis of the 1D two-particle Schrödinger equation [26]

$$[(\hbar^2/2\mu)\nabla^2 + |e|Ez + F]\Phi(r) = 0, \quad (19)$$

where E is the electric field in the Z direction, F is the sum of the electron and hole energies measured from their respective band edges, and μ is the reduced mass that is defined by

$$\frac{1}{\mu} = \frac{1}{m_h^*} + \frac{1}{m_e^*}. \quad (20)$$

As an example, we set the bias equal to 2 V. We assume that the electric field in the intrinsic is uniform, and the strength of the electric field should be approximately 1×10^7 V/m. Equation (18) then implies $l_A = 5.04 \times 10^{-9}$ m. Figure 10(a) shows $(1/E)(dE/dz)$ in the intrinsic region. We see the Eq. (17) is always satisfied. Figure 10(b) shows the electric field in the device as a function of z . We can see that the electric field is almost zero in the p -region except at the interface between the different layers.

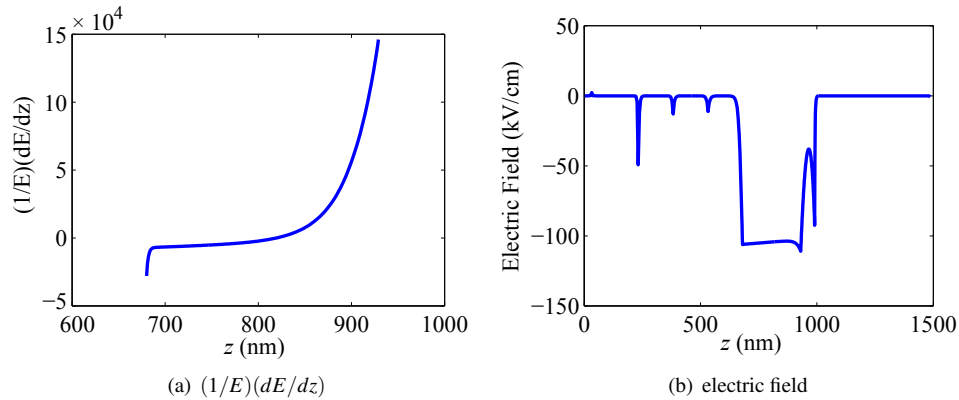


Fig. 10. (a) The function $(1/E)(dE/dz)$ in the intrinsic region. (b) The electric field distribution in the device in the z -direction.

5.3. History-dependent impact ionization

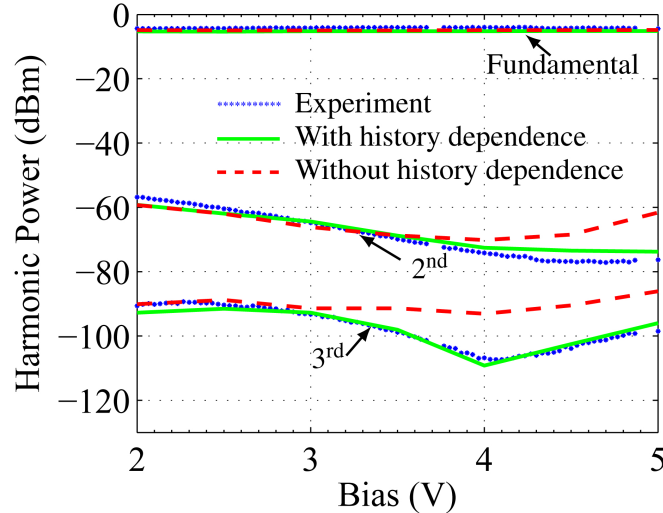


Fig. 11. Calculated harmonic powers when we use the impact ionization Eq. (12), which has no history dependence

Figure 11 shows calculated harmonic powers when we use the local field-dependent impact ionization given in Eq. (12), which does not take the dead length into account. The local field-dependent impact ionization overestimates the impact ionization coefficient in the device.

Since the intrinsic region of this photodetector is only 250 nm, the dead length effect [8] cannot be ignored, and we must use a history-dependent ionization.

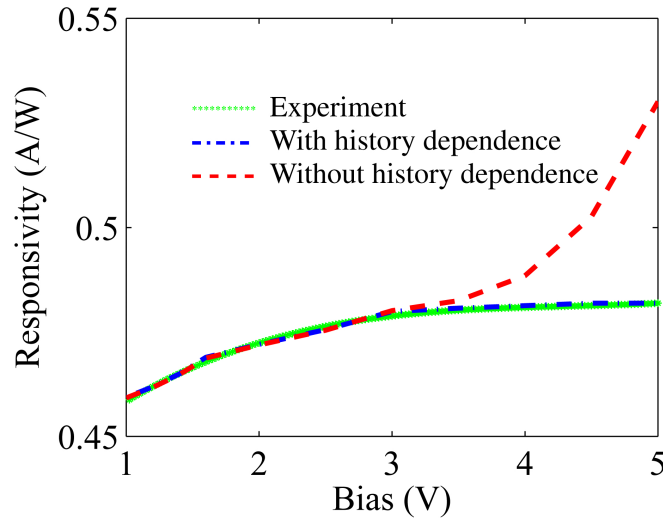


Fig. 12. Calculated responsivity of the photodetector in our 2D simulation. The green stars show the experimental results, the blue dash-dot curve shows the simulated result with history-dependent impact ionization, and the red dashed curve shows the simulated result without history-dependent impact ionization. The output current is 9 mA. The incident light wavelength is 1550 nm.

Figure 12 show the responsivity using the local field-dependent impact ionization. When the history dependence is not included and the bias is greater than 4 V, we find that the calculated responsivity is higher than the experimental responsivity. Our simulations show the impact ionization does not make an important contribution to nonlinearity in this device, which is consistent with the results in [10]. However, without using the history-dependent impact ionization in the simulation, the model will overstate the importance of the impact ionization. Thus it is important to use the history dependent impact ionization in order to accurately determine the importance of this effect.

5.4. Suggestions for improving device performance

The Franz-Keldysh effect in the intrinsic region is an important source of nonlinearity in this photodetector. It plays almost no role in the other device regions, because the electric field is nearly zero outside the intrinsic region and does not change with the photo-generated carriers. It is therefore advantageous to maximize the absorption in the p -region, which may be done by increasing its length. The absorption in the intrinsic region decreases for the same output photocurrent when the length of the p -region absorption layers increases. The change of the electric field in the intrinsic region due to the photo-generated carriers decreases. So, the nonlinearity in the intrinsic region decreases. Figure 13(a) shows the calculated harmonic powers when we double the length of the p -region absorption layers. The harmonic powers decrease by about 5 dB between 2 and 4 V. These curves are similar to the simulation results without the Franz-Keldysh effect, as shown in Fig. 8(a).

Figure 13(b) shows the calculated harmonic powers when we double the length of intrinsic region. The strength of the electric field decreases when the length of intrinsic region increases, increasing the period of the Franz-Keldysh oscillations in the absorption coefficient. We find

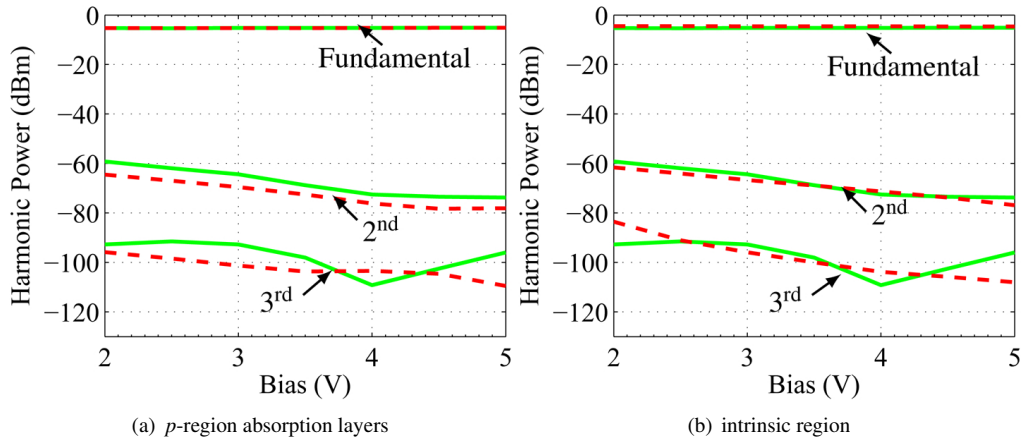


Fig. 13. Calculated harmonic powers when we double the length of (a) the *p*-region absorption layers (red dashed curves) and (b) the intrinsic region (red dashed curves). For comparison, we also show the original calculation as green solid curves.

that the harmonic powers decreases somewhat at high bias when we increase the length of the intrinsic region.

Figure 8(b) indicates that the third harmonic power decreases without the load resistor. It is not possible in practice to make the load resistance zero. However, we note that the photodetector is close to an ideal current source and operates most linearly with a fixed bias across the device. For narrowband applications, it is possible to use impedance matching to reduce the effective load resistance and increase the linearity of the device. Figure 14 shows the calculated harmonic powers with differing load resistances. We are assuming that an impedance-matching circuit is used to match the effective load resistance to the final load, which is held at $50\ \Omega$, so that the power dissipation is given by $\frac{1}{2}I^2 \times 50\ \Omega$. Decreasing the effective load resistor decreases the third harmonic power significantly at biases below 4 V.

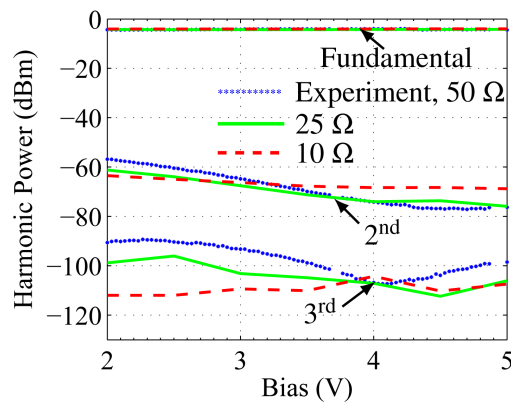


Fig. 14. Calculated harmonic powers with effective load resistances of 10 and 25 Ω .

Another possibility that we considered to reduce the impact of the Franz-Keldysh effect is to increase the so-called “unintentional” doping density in the intrinsic region. Figure 15 shows the calculated harmonic powers when we increase the doping density from 1×10^{15} to

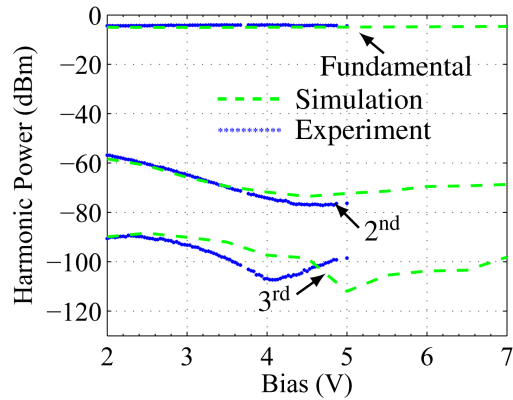


Fig. 15. Calculated harmonic powers when the doping density in the intrinsic region increases from 1×10^5 to $5 \times 10^5 \text{ cm}^{-3}$.

$5 \times 10^{15} \text{ cm}^{-3}$. We find that the second harmonic power is almost the same. The dip in the third harmonic power shifts from 4 V to around 5 V. However, we do not see any decrease in the harmonic powers. A possible reason is that the dark current increases when the doping density in the intrinsic region increases. So, this approach does not succeed for this structure.

6. Conclusion

We have developed a 2D drift-diffusion model to study nonlinearity and harmonic power generation in a PDA photodetector. The heat flow equation was included in the model to study the effects of temperature change as a function of bias. We have shown that it is necessary to take into account history dependence of the impact ionization in this PDA photodetector, which has a thin intrinsic region. Without history-dependent impact ionization, the effect of impact ionization is overestimated and we cannot obtain agreement with the experiment for either the responsivity or the harmonic powers. We also achieved excellent agreement with the experiments at different modulation frequency.

We found that the Franz-Keldysh effect plays an important role in the device nonlinearity. We can mitigate the effect of the Franz-Keldysh effect by increasing the length of the *p*-region absorption layers. The change of the absorption coefficient principally occurs in the intrinsic region. The absorption in the *p*-region absorption layers remains the same because the electric field does not change with the incident light power. Increasing the length of the *p*-region absorption layers therefore decreases the nonlinearity due to the Franz-Keldysh effect.

It would be helpful to measure the output photocurrent with a fixed applied voltage across the device. With the load resistor in the measured circuit, it is difficult to fix the voltage across the device when the photocurrent changes. However, the harmonic powers decrease when we decrease the effective load resistance. The third harmonic power decreases by more than 10 dB when the effective load resistance is 10Ω .

Acknowledgment

Work at UMBC was partially supported by the Naval Research Laboratory. The 2D simulations were carried out at UMBC's high performance computing facility.